RESSALVA

Atendendo solicitação do(a) autor(a), o texto completo desta tese será disponibilizado somente a partir de 09/11/2018.

Development of glass optical fibers based on fluoride-phosphate for deep-UV optical transmission

Thèse en cotutelle
Doctorat en chimie

Gustavo Galleani

Université Laval
Québec, Canada
Philosophiae Doctor (Ph. D.)

et

Universidade Estadual Paulista "Júlio de Mesquita Filho"
Araraquara, Brasil
Doutorado

GUSTAVO GALLEANI

Development of glass optical fibers based on fluorophosphate for deep-UV optical transmission

Thesis in co-title with Université Laval – Quebec – Canada presented to the Institute of Chemistry, Universidade Estadual Paulista, to obtain the degree of Doctor in Chemistry

Brazilian advisor: Younes Messaddeq
Brazilian co-advisor: Silvia Helena Santagneli
Canadian advisor: Denis Boudreau

Araraquara
2017

FICHA CATALOGRÁFICA

Galleani, Gustavo
G166d Development of glass optical fibers based on fluoride-phosphate for deep-UV optical transmission / Gustavo Galleani. – Araraquara: [s.n.], 2017
182 p.: il.

Thesis (doctor) – Universidade Estadual Paulista, Instituto de Química
Advisor: Younes Messaddeq
Advisor: Denis Boudreau
Co-advisor: Silvia Helena Santagneli

1. Glass. 2. Nuclear magnetic resonance. 3. UV spectrum. 4. Raman spectroscopy. 5. Luminescence. I. Title.

Elaboração: Seção Técnica de Aquisição e Tratamento da Informação
Biblioteca do Instituto de Química, Unesp, câmpus de Araraquara

UNIVERSIDADE ESTADUAL PAULISTA

Câmpus de Araraquara

CERTIFICADO DE APROVAÇÃO

TÍTULO DA TESE: "Development of glass optical fibers based on fluorophosphate for deep-UV optical transmission"

AUTOR: GUSTAVO GALLEANI
ORIENTADOR: YOUNES MESSADDEQ
COORIENTADORA: SILVIA HELENA SANTAGNELI
COORIENTADOR: DENIS BOUDREAU

Aprovado como parte das exigências para obtenção do Título de Doutor em QUÍMICA, pela Comissão Examinadora:

Prof. Dr. YOUNES MESSADDEQ
Departamento de Química Geral e Inorgânica / Instituto de Química - UNESP - Araraquara

VIDEOCONFERÊNCIA

Prof. Dr. DENIS BOUDREAU
Département de Chimie / Faculté des Sciences et de Génie - Université Laval - Québec

Prof. Dr. MARCELO NALIN
Departamento de Química Geral e Inorgânica / Instituto de Química - UNESP - Araraquara

Prof. Dr. HELLMUT ECKERT
Departamento de Físico-Química / Instituto de Química - USP - São Carlos

VIDEOCONFERÊNCIA

Prof. Dr. MARTIN BERNIER
Département de Physique / Faculté des Sciences et de Génie - Université Laval - Québec

UNIVERSIDADE ESTADUAL PAULISTA

Câmpus de Araraquara

VIDEOCONFERÊNCIA

Prof. Dr. THIERRY CARDINAL
Chimie et Photonique des Matériaux Oxydes et Fluorures / Institut de Chimie de la Matière Condensée de Bordeaux - Pessac - France

Araraquara, 09 de novembro de 2017

unesp

UNIVERSIDADE ESTADUAL PAULISTA

Câmpus de Araraquara

Instituto de Química

CERTIFICADO DE APROVAÇÃO

TÍTULO DA TESE: "Development of glass optical fibers based on fluorophosphate for deep-UV optical transmission"

AUTOR: GUSTAVO GALLEANI
ORIENTADOR: YOUNES MESSADDEQ
COORIENTADORA: SILVIA HELENA SANTAGNELI
COORIENTADOR: DENIS BOUDREAU

Aprovado como parte das exigências para obtenção do Título de Doutor em QUÍMICA, pela Comissão Examinadora:

Prof. Dr. YOUNES MESSADDEQ
Departamento de Química Geral e Inorgânica / Instituto de Química - UNESP - Araraquara

Prof. Dr. DENIS BOUDREAU
Département de Chimie / Faculté des Sciences et de Génie - Université Laval - Québec

Prof. Dr. MARCELO NALIN
Departamento de Química Geral e Inorgânica / Instituto de Química - UNESP - Araraquara

Prof. Dr. HELLMUT ECKERT
Departamento de Físico-Química / Instituto de Química - USP - São Carlos

Prof. Dr. MARTIN BERNIER
Département de Physique / Faculté des Sciences et de Génie - Université Laval - Québec

unesp

UNIVERSIDADE ESTADUAL PAULISTA

Câmpus de Araraquara

Prof. Dr. THIERRY CARDINAL
Chimie et Photonique des Matériaux Oxydes et Fluorures / Institut de Chimie de la Matière Condensée de Bordeaux - Pessac - France

Araraquara, 09 de novembro de 2017

RÉSUMÉ

Le développement de nouvelles fibres optiques capables de transmettre dans les régions de l'ultraviolet moyen (200-300 nm) et lointain (120-200 nm) bénéficierait aux techniques de microlithographie, aux technologies laser, et également à la détection chimique (détection du phosphore et du soufre pour l'agriculture), ce qui représent la principale motivation de ce travail. En outre, les verres mixtes fluorure/phosphate peuvent offrir un environnement de fluorures de faible énergie de phonons qui est favorable pour l'émission avec une grande efficacité quantique lorsqu'ils sont dopés avec des ions de terre rare trivalents. Une telle propriété rend alors leur utilisation attractive pour d'autres applications également sous forme de fibres et/ou verres massifs dans le domaine de la photonique.

La seule fibre connue pouvant opérer dans l'UV (~170-300 nm) est constituée de silice pure dopée avec OH/F. Cependant, l'utilisation de telles fibres est limitée par l'effet de solarisation qui dégrade la transmission de la lumière UV après une exposition prolongée.

Les verres à base de *fluorophosphate* (FP) sont des matériaux hautement transparents dans l'UV lorsqu'ils possèdent de faibles quantités d'impuretés, offrant ainsi une alternative aux fibres de silice utilisées aujourd'hui dans cette région du spectre électromagnétique. Ces verres sont produits par le mélange de fluorures et polyphosphates et combinent ainsi leurs propriétés telles que: une excellente aptitude à vitrifier, un faible indice de réfraction et une large fenêtre de transmission (~ 160-4000 nm). Toutefois, peu d'études ont été rapportées à ce jour sur leur méthode de fabrication et par conséquent, les pertes optiques dans la région UV. En outre, lorsqu'il est dopé avec des ions de terres rares trivalentes (RE), l'environnement de faible énergie de phonon est favorable pour les efficacités quantiques élevées, ce qui permet une application photonique sous forme de fibre et/ou de verre massif.

Par conséquent, des verres FP très purs ont été préparés et utilisés pour fabriquer des fibres optiques à saut d´indice, par une technique de creuset modifiée. Dans une première étape, les verres ont été étudiés pour être très transparents dans la région VUV, jusqu'à 160 nm, et les caractéristiques des températures, la viscosité autour du point de ramollissement ont été caractérisées. Ensuite, les fibres ont été fabriquées par la technique du creuset, par l´étirage d´une préforme à travers un creuset en silice fondue. Alors que la cristallisation incontrôlée a été observée lors du tirage des fibres par le procédé classique, l'étirage à partir

d'un creuset en silice fondu s'est avéré approprié pour obtenir des fibres de verre FP exemptes de cristaux. Ensuite, des mesures d'atténuation ont été effectuées sur les fibres.

La deuxième partie de cette thèse est compose de deux parties: l'étude structurale des verres FP avec différent ratios fluorure/phosphate et la corrélation des propriétés luminescentes des verres dopés avec des ions de terres rares avec leur structure. Les verres obtenus ont été caractérisés par différentes techniques, calorimétrie différentielle à balayage (DSC), spectroscopie Raman et résonance magnétique nucléaire à l'état solide (RMN). Au cours de l'étape suivante, on a utilisé des techniques de double resonance $^{27}Al/^{31}P$ pour quantifier le nombre moyen de liaisons P-O-Al dans les verres et l'environnement local des espèces de fluorure a également été déterminé. Ensuite, les verres ont été dopées avec des ions de terres rares et l'environnement local a été caractérisé par spectroscopie de résonance paramagnétique électronique (RPE) de la sonde Yb^{3+} et par des expériences de photoluminescence sur des ions Eu^{3+}. Les propriétés de la luminescence ont été corrélées avec la transformation structurale en fonction de la composition.

Enfin, en raison de la haute transparence UV, nous avons préparé des verres FP dopées avec des ions Gd^{3+}, Tm^{3+} et Yb^{3+} comme candidat potentiel pour la fabrication de lasers à fibre UV. Les propriétés de photoluminescence sous excitation au laser à diode de 980 nm ont été étudiées et l'effet des différent ratios fluorure/phosphate dans les verres sur l'émission de conversion ascendante UV du Gd^{3+} a egalement été etudié. Ensuite, leurs propriétés structurales ont également été explorées par la résonance magnétique nucléaire du ^{45}Sc, incorporé pour imiter les ions de terres rares dans la matrice vitreuse.

En utilisant la technique de la double résonance $^{45}Sc/^{31}P$, la distribution du ligand entourant les ions de terres rares a été quantifiée et l'efficacité de l'émission du Gd^{3+} par rapport aux ions Tm^{3+} avec la structure a été effectuée.

ABSTRACT

The development of new optical fibers capable to operate in the deep-ultraviolet (DUV, 200-300 nm) and the vacuum-ultraviolet (VUV, 120-200 nm) would benefit to laser technologies, microlithography techniques (increased spatial resolution) and elemental chemical sensing applications (phosphorous and sulfur sensing in agriculture).

The only well-established UV-transmitting fiber existing to date consists in high-OH/fluorine doped silica glass core/clad fibers. However, the utilization of such fibers is limited by solarisation effect that degrades the UV-light transmission with long time exposition.

Mixed fluoride-phosphate (FP) glasses with ultra-low content of impurities can be VUV- and/or DUV-transmitting materials, offering thus an alternative to the commercialized high-OH/fluorine doped silica fibers. These glasses are produced by mixing fluorides and polyphosphates to combine their properties as excellent glass-forming ability, low refractive index and broad optical transmission windows ranging from ~160 to 4000 nm. Also, when doped with trivalent rare-earth (RE) ions, the low phonon fluorine environment is favorable for RE high quantum efficiencies, making then suitable for photonic application in the form of fiber and/or bulk glass.

Firstly, highly pure FP glasses were prepared and utilized to fabricate step-index optical fibers, by a modified crucible technique. In a first step, the bulk glasses were studied to be highly transparent in the VUV region, down to 160 nm, and the characteristics temperatures, viscosity around softening point were characterized. Then, the fibers were fabricated by the crucible technique, drawing the as-made core-cladding preforms in a silica crucible assembly. While uncontrolled crystallization was observed during the fiber drawing by the conventional method, drawing from a fused silica crucible showed to be suitable to obtain crystal-free FP glass fibers. Additionally, the cut-back method was employed to measure the optical attenuation on the FP step-index and single index glass fibers.

The second part of this thesis involves the network structural investigation of a series of FP glasses with different fluoride/phosphate ratio. Raman and multinuclear solid-state nuclear magnetic resonance (NMR) spectroscopies were used to study the polyphosphate network transformation for the different fluoride/phosphate ratios. In the next step $^{27}Al/^{31}P$

double resonance techniques were used to quantify the average number of P-O-Al linkages in the glasses and the local environment of fluoride species were also determined. Then, the glasses were doped with RE ions and the local environment was characterized by electron paramagnetic resonance (EPR) spectroscopy of Yb^{3+} ions probe and by photoluminescence experiments on Eu^{3+} dopant ions. The luminescence properties were correlated with the structural transformation as a function of composition.

Lastly, due to the high UV tansparency of the FP glasses, we prepared FP glasses doped with Gd^{3+}, Tm^{3+}, and Yb^{3}+ ions as a potential candidate for fabrication of UV fiber lasers. The photoluminescence properties under 980 nm diode laser excitation were studied, and the effect of fluoride/phosphate ratio in the glasses in the Gd^{3+} UV upconversion (UC) emission were verified. The effect of Gd^{3+} content in the UV UC emission was also studied. Then, by using $^{45}Sc/^{31}P$ double resonance technique, utilizing scandium as a diamagnetic mimic for the luminescent RE species, the ligand distribution surrounding the RE ions were quantified, and the efficiency of the Gd^{3+} emission, compared to the Tm^{3+} ions with structure was done.

RESUMO

O desenvolvimento de novas fibras ópticas capazes de operar na região do ultravioleta profundo (200-300 nm) e de vácuo (120-200 nm) beneficiariam aplicações em tecnologias a laser, técnicas de microlitografia (maior resolução espacial) e detecção química elementar (detecção de fósforo e enxofre na agricultura).

A única fibra de transmissão UV bem estabelecida existente até o momento consiste em fibras núcleo-casca de vidro de sílica dopado com OH/flúor. No entanto, a utilização de tais fibras é limitada pelo efeito de solarização que degrada a transmissão da luz UV apos exposição prolongada.

Os vidros mistos fluoreto-fosfato com baixas quantidades de impurezas, são materiais transmissores de luz UV-profundo e vácuo, oferecendo assim uma alternativa frente as fibras de silica utilizadas hoje. Estes vidros são produzidos pela mistura de fluoretos e polifosfatos com propriedades combinadas de ambos como, excelente capacidade de formação vítrea, baixo índice de refração e ampla janela de transmissão (~ 160 a 4000 nm). Além disso, quando dopados com íons terras-raras trivalentes, o ambiente de baixa energia de fonon dos fluoretos é favorável para emissões dos TRs com alta eficiência quântica, tornando-os então adequados para aplicações na área da fotônica na forma de fibra e/ou bulk.

Portanto, em primeiro lugar, foram preparados vidros FP altamente puros e utilizados para fabricação de fibras ópticas de índice-degrau, pela técnica do cadinho. Na primeira etapa, os vidros na forma de bulk foram estudados para serem altamente transparentes na região ultravioleta de vácuo, até 160 nm, e suas temperaturas características e a viscosidade em torno do ponto de amolecimento foram caracterizadas. Em seguida, as fibras foram fabricadas pela técnica do cadinho, preparando as preformas núcleo-casca em um conjunto de cadinho de sílica. Embora a cristalização não controlada tenha sido observada durante o puxamento das fibras pelo método convencional, o puxamento pelo método do cadinho mostrou-se adequado para obtenção de fibras de vidro FP sem cristalização. Além disso, a atenuação óptica nna fibra obtida foi medida na região UV.

A segunda parte desta tese envolveu a investigação estrutural de uma série de vidros FP com diferentes razoes fluoreto/fosfato. As espectroscopias RMN do estado solido e Raman foram utilizadas para estudar a transformação da rede de polifosfatos para as

diferentes razoes fluoreto/fosfato. Na etapa seguinte, utilizaram-se técnicas de dupla ressonância do $^{27}Al/^{31}P$ para quantificar o número médio de ligações P-O-Al nos vidros e o ambiente local das espécies fluoreto também foi determinado. Em seguida, os vidros foram dopados com íons TRs e o ambiente local foi caracterizado por espectroscopia EPR da sonda de íons Yb^{3+} e por medidas de fotoluminescência dos íons Eu^{3+}. As propriedades de luminescência foram correlacionadas com a transformação estrutural em função da composição.

Por último, devido à elevada transparência UV dos vidros FP, preparamos vidros FP dopados com íons Gd^{3+}, Tm^{3+} e Yb^{3+} como potencial candidato para fabricação de fibras laser UV. As propriedades de fotoluminescência sob excitação laser de diodo de 980 nm foram estudadas e o efeito da razão fluoreto/ fosfato nos vidros na emissão UV do íon Gd^{3+} por conversão ascendente de energia foi verificado. O efeito da concentração de Gd^{3+} nesta emissão também foi estudado. Em seguida, utilizando a técnica de ressonância dupla $^{45}Sc/^{31}P$, com o escândio como um mímico diamagnético para as espécies de terras-raras luminescentes, a distribuição dos ligantes no ambiente de coordenação dos íons TRs foi quantificada e a eficiência da emissão do Gd^{3+}, em comparação com as emissões do íon Tm^{3+} com a estrutura foi feita.

1. TABLE OF CONTENTS

RÉSUMÉ……..…….....vi

ABSTRACT……...…...…….…viii

RESUMO…….……....xi

TABLE OF CONTENTS……..……..xii

LIST OF FIGURES……...…….…....xv

ACKNOWLEDGEMENT…….....xx

FOREWORD……...……..xxii

THESIS SYNOPSES……...…….....xxiv

1. INTRODUCTION 1

1.1. Materials with (large and) extended transparency in the UV *2*

1.1.1. Fluoride crystals and vitreous silica as materials for UV optics *3*

1.1.2. Mixed fluoride-phosphate glasses *3*

1.1.3. Deep-UV fiber and radiation induced defects *6*

1.2. State of the art: general consideration on glasses 8

1.2.1. Glass definition *8*

1.2.2. Glass transition temperature (Tg) *9*

1.2.3. Glass optical properties *10*

1.2.4. Reflection *11*

1.2.5. Refractive index *12*

1.2.6. Transmission window *13*

1.3. Fundamental aspects of optical fibers 14

1.3.1. Propagation in a conventional step-index fiber *14*

1.3.2. Modes of propagation *16*

1.3.3. Optical losses in the fiber *17*

1.3.3.1. Intrinsic optical absorption *18*

1.3.3.2. Extrinsic optical absorption *18*

1.3.4. Prediction of loss minima *19*

1.4. Fundamental aspects of solid-state NMR....20
1.4.1. The basic interactions in solid-state NMR....20
1.4.1.1. The zeeman effect....20
1.4.1.2. Chemical shielding – chemical shift interaction....21
1.4.1.3. Dipolar coupling....22
1.4.1.4. Scalar coupling (J-couplin) 23
1.4.1.5. Eletric quadrupolar coupling....23
1.4.2. Methods of NMR spectroscopy....24
1.4.2.1. Magic angle spinning (MAS) 24
1.4.2.2. Static dipolar NMR spectroscopy....25
1.4.2.3. Rotational echo double resonance - REDOR....26.
2. OBJECTIVES....28
3. UV-TRANSMITTING STEP-INDEX FLUOROPHOSPHATE GLASS FIBER FABRICATED BY THE CRUCIBLE TECHNIQUE 29
3.1. Introduction....31
3.2. Experimental procedure....33
3.2.1. Bulk glass synthesis....33
3.2.2. Core-cladding preform preparation and optical fiber drawing:....34
3.3. Material characterization....36
3.3.1. Thermal characterization: 36
3.3.2. Optical Characterization:....37
3.4. RESULTS AND DISCUSSION 37
3.4.1. Bulk glasses characterization. 37
3.5. Conclusion 51
3.6. References....52
4. RARE-EARTH DOPED FLUORIDE PHOSPHATE GLASSES: STRUCTURAL FOUNDATIONS OF LUMINESCENCE PROPERTIES....55
4.1. Introduction....57
4.2. Experimental procedure....59
4.2.1. Bulk glass synthesis: 59
4.2.2. Glass sample characterization: 60

4.2.3. Solid state NMR. 61
4.2.4. Solid state EPR: 63
4.3. Results, data analysis and interpretation 64
4.3.1. Glass Properties..... 64
4.3.2. Raman Spectroscopy. 64
4.3.3. Solid state NMR. 65
4.3.3.1. Single-pulse NMR. 65
4.3.3.2. $^{31}P\{^{27}Al\}$ REAPDOR and $^{19}F\{^{31}P\}$ and $^{27}Al\{^{31}P\}$ REDOR. 69
4.3.4. Photophysical characterization on Eu^{3+} fluoride-phosphate glass samples. 73
4.3.5. Pulsed EPR Spectroscopy on Yb^{3+}-doped fluoride-phosphate glass samples. 77
4.4. Conclusions 83
4.5. References 84
5. ULTRAVIOLET UPCONVERSION LUMINESCENCE IN A HIGHLY TRANSPARENT TRIPLY-DOPED Gd^{3+}-Tm^{3+}-Yb^{3+} FLUORIDE-PHOSPHATE GLASSES. 89
5.1. Introduction 92
5.2. Experimental Procedure 94
5.2.1. Bulk glass synthesis: 94
5.2.2. Glass sample characterization. 95
5.3. Results and discussion 95
5.4. Conclusion 111
6. GENERAL CONCLUSION 116
RESUMO EXPANDIDO DA TESE EM PORTUGUÊS. 118
RÉSUMÉ COMPLET DE LA THÈSE 137
REFERENCES……...……...153

LIST OF FIGURES

Figure 1-1. Schematic representation of Q^n phosphate tetrahedral units. 5

Figure 1-2. Variation of the specific volume with temperature. Adapted from (ZARZYCKI, 1982). (l – liquid; sl – super-cooled liquid; c – crystal; v - glass.....9

Figure 1-3. Refraction of light phenomenon in the passage through two homogeneous isotropic media of respective refractive indices n_1 and n_2. Adapted from (Bach et al., 1998) 12

Figure 1-4. Example of transmission window for different classes of glass adapted from (NALIN et al., 2016).....14

Figure 1-5. Schematic figure of a conventional optical fiber. 15

Figure 1-6. Schematic of light-ray propagation in multimode step-index, graded-index (b) and single-mode optical fiber. Adapeted from fiber optic share website (www.fiberopticshare.com) 16

Figure 1-7. V-curve due to intrinsic optical absorption high grade silica fiber. Adapted from (MIMURA; NAKAI, 1991) 19

Figure 1-8. The magic angle orientation of 54.7°relative to the direction of the static field (B_0)……25

Figure 3-1. Fused silica crucible assembly used for fiber drawing.....36

Figure 3-2. DSC curves of the studied fluorophosphate glasses $xBa(PO_3)_2$-90-x(AlF_3, CaF_2, MgF_2, SrF_2), x = 5, 10 and 20 mol%, respectively labelled as 5BaPF95, 10BaPF90 and 20BaPF80…….....39

Figure 3.3. (a) Deep-UV and (b) infrared transmission spectra, for the core and cladding glasses with 1.50 and 1.70 mm thickness, respectively……...40

Figure 3-4. Dispersion curves for the core (10BaPF90, red line) and cladding (10SrPF90, black line) glass compositions, determined from ellipsometry measurements…….42

Figure 3-5. Photographs of the cladding glass tube (a) and the core glass rod (b).....43

Figure 3-6. DSC traces and viscosity recorded by the parallel plate method as a function of temperature of the core (10SrPF90, black line) and cladding (10BaPF90, red line) glass compositions. The heating rate was 10˚C/min for the thermal analysis and 2˚C/min for the viscosity measurement…….....44

Figure 3-7. Photograph of the fabricated optical fiber (a). Optical microscopy image of the optical step-index fiber section (127 μm diameter) without polymer coating (b)……..…45

Figure 3-8. Measured power output at 244 nm wavelength, recorded from a fiber initial section of 0.2 m. In red: best fit of the attenuation curve, weighted to the linear intensity of the signal…….....47

Figure 3-9. Attenuation spectra of the single-index fiber (red curve) and core-cladding fiber (black curve) measured by the cut-back method on 3 fiber sections…….……...48

Figure 4-1. Raman spectra of the fluoride-phosphate glasses…….……49

Figure 4-2. (a) Experimental single-pulse ^{31}P MAS NMR spectra and deconvolution model (b) Refocused INADEQUATE (red traces) and single pulse ^{31}P MAS NMR spectra (black traces) of the investigated fluoride-phosphate glasses. Amplitudes of the black and red traces are chosen arbitrarily, and cannot be compared to each other…….……..…...65

Figure 4-3. ^{27}Al MAS NMR spectra of the investigated fluoride-phosphate glasses (black curves). Red curves represent simulations of the data using the Czjzek model…….….66

Figure 4-4. ^{19}F-MAS NMR spectra of the investigated fluoride-phosphate glasses. Dashed colored curves denote the deconvolutions into individual Gaussian components. Black curves denote experimental data. Spinning sidebands are marked with asterisks……..……..68

Figure 4-5. 19F{31P} REDOR results for the glasses under study. a) REDOR curves for the -95 ppm and b) Redor curves for the -135 ppm resonances (right). Solid curves show parabolic fits to the initial data range $\Delta S/S0 \leq 0.2$. Squares represent experimental points……..……...69

Figure 4-6. $^{27}Al\{^{31}P\}$ REDOR dephasing curves for the set of fluoride-phosphate samples. Circles represent experimental points obtained under MAS spinning speeds of 14.0 and 12.0 kHz. Solid curves are parabolic fits to the data, analyzed within the data range of $\Delta S/S0 \leq 0.2$……..……70

Figure 4-7. $^{31}P\{^{27}Al\}$ REAPDOR dephasing curves of the investigated for fluoride-phosphate glasses. The curves represent SIMPSON simulations of the REAPDOR curves for ^{31}P interacting with 1 (solid black curve), 1.3 (dashed blue curve) or 2 (dashed red curve) ^{27}Al neighbors at a distance of 3.27 Å……..…….71

Figure 4-8. Visible emission spectra obtained of the 0.5 mol % Eu^{3+} containing fluoride-phosphate glass samples. The spectra are internally normalized to the peak intensity at 595 nm ($^5D_0 \rightarrow {}^7F_1$). The label 5SrF_05Eu_bif indicates the sample prepared with excess NH_4HF_2 present in the melt…..……73

Figure 4-9. Photoluminescence excitation (PLE) spectra by monitoring the $^7F_2 \rightarrow {}^5D_0$ transition at 611 nm. The inset shows the internally normalized phonon sideband transition at around 441 nm. The label 5SrF_05Eu_bif indicates the sample prepared with excess NH_4HF_2 present in the melt.....74

Figure 4-10. Decay curves obtained obtained for 0.5 mol % Eu^{3+} containing fluoride-phosphate glass samples for the $^5D_0 \rightarrow {}^7F_2$ (λexc = 464 nm) of Eu^{3+} dopants. The label 5SrF_05Eu_bif indicates the sample prepared with excess NH_4HF_2 present in the melt……..……..……....76

Figure 4-11. Echo-detected field-sweep (EDFS) EPR spectra for Yb-doped glasses (The label 5SrPFB represents the sample prepared with excess NH_4HF_2 present in the melt)…… ……..……..…..77

Figure 4-12. Center of gravity of the EDFS spectra taken in the magnetic field region 0.1 – 10 kG, for the glasses studied in the present work and for fluoride-phosphate glasses reported in the literature,[20,21] as a function of the P/F molar ratio (a) and as a function of the photophysical parameters α and τ. The code 5SrPFB denotes the sample melted in the presence of excess ammonium bifluoride……..78

Figure 4-13. Three-pulse ESEEM spectra for the studied glasses. The code 5SrPFB denotes the sample melted in the presence of excess ammonium bifluoride. The spectra were recorded at magnetic field strength of 700 mT. Each spectrum was obtained from the co-addition of spectra for τ = 100 ns, 120 ns and 140 ns (τ is the first delay in the three-pulse sequence), resulting in blind-spot-free spectra. Resonances are marked with the correspondent nuclear species…….……..……79

Figure 4-14. $^{31}P/^{19}F$ ESEEM peak intensity ratios $I(^{31}P)/I(^{19}F)$ as a function of the P/F ratio of the batch for the glasses studied in the present work (red triangles) compared with data from the glass system $25BaF_2$-$25SrF_2$-$(30-x)Al(PO_3)_3$-$xAlF_3$-$20MF_3$, where M = Y (blue triangles)[21] or Sc (black circles).[20] Dashed lines are drawn as guide to the eyes……..……80

Figure 4-15. 2D-HYSCORE spectra recorded at a magnetic field strength of 500 mT for the studied glasses The code 5SrPFB denotes the sample melted in the presence of excess ammonium bifluoride. The anti-diagonal dashed lines cross the diagonal at the nuclear Zeeman frequencies for the isotopes indicated in the plots. A simulation considering one ^{27}Al, one ^{31}P and two ^{19}F species interacting with the electron spin through the hyperfine interaction is also shown. The simulation parameters are described in the text…….81

Figure 5-1. (a) Single-pulse ^{31}P MAS-NMR and (b) ^{27}Al MAS-NMR spectra of the 5PF6Sc and 10PF6Sc fluoride-phosphate glasses…..……....98

Figure 5-2. $^{27}Al\{^{31}P\}$ REDOR dephasing curves for the 5PF6Sc and 10PF6Sc glass samples and crystalline $Al(PO_3)_3$. Squares represent experimental data obtained under MAS spinning speeds of 14.0 and 12.0 kHz. Solid curves are parabolic fits to the data, analyzed within the data range of $\Delta S/S_0 \leq 0.2$…….....99

Figure 5-3. $^{31}P\{^{27}Al\}$ REAPDOR dephasing curves of the investigated fluoride-phosphate glasses. The solid red curve represents SIMPSON simulations of the REAPDOR curves for ^{31}P interacting with two ^{27}Al neighbors at a distance of 3.27 Å……..…….....101

Figure 5-4. ^{19}F-MAS-NMR spectra of the 5PF6Sc and 10PF6Sc fluoride-phosphate glasses. Dashed colored curves denote the deconvolutions into individual Gaussian components. Black curves denote experimental data. Spinning sidebands are marked with asterisks……..……102

Figure 5-5. ^{45}Sc MAS-NMR spectra for the glasses 5PF6Sc and 10PF6Sc and crystalline ScF_3…….…….…….…….103

Figure 5-6. $^{45}Sc\{^{31}P\}$ REDOR dephasing curves of the 5PF6Sc and 10PF6Sc glasses. Squares represent experimental points obtained under MAS spinning speeds of 12.0 kHz Solid curves are parabolic fits to the data, analyzed within the data range $\Delta S/S_0 \leq 0.2$……..…….....104

Figure 5-7. Absorption spectra obtained for the undoped and Gd^{3+}-Tm^{3+}-Yb^{3+} fluoride-phosphate glasses. Assignments of RE^{3+} absorption bands are shown in the figure. (The spectra have been vertically translated for better comparison) …….…...106

Figure 5-8. Upconversion emission spectrum under 200 mW 980 nm laser excitation for the representative glass sample 10PF4Gd. Assignments are shown in the figure…….….107

Figure 5-9. Energy level diagrams of Gd^{3+}, Tm^{3+} and Yb^{3+} ions with the possible upconversion process adapted from Ref. [47]. CR cross-relaxation; ET energy transfer……..……...109

Figure 5-10. Ultraviolet upconversion spectra under 400mW 980 nm laser excitation of the fluoride-phosphate glass samples as a function of: (a) the Gd^{3+} content and (b) the fluoride/phosphate ratio. Spectra are normalized by the Tm^{3+} : $^1I_6 \rightarrow {}^3H_6$ (290 nm) band intensity. Assignments are shown in the figure. ……...……..….110

Figure 5-11. (a) Power dependence and (b) Log-log plot of the UV UC emissions at 290, 310 and 360 nm excited by 980 nm laser for the representative sample 10PF2Gd……..…….……..111

I dedicated this thesis to my family and friends, in whom I admire and love and have always supported me in this journey.

ACKNOWLEDGMENTS

I would like to thank those had a direct and indirect impact in my studies during these last 4 years.

I am glad of had been advised by Prof. Dr. Younes Messaddeq, who I admire for his expertise and enthusiasm. I am deeply grateful for all support, guidance, discussions and opportunities, which were essentials to my progress and learning.

Dr. Yannick Ledemi has also been an important person during all my PhD, as important as Prof. Dr. Younes Messaddeq himself. Thank you for all discussions, suggestions and teaching about science and also the valuable advices for life.

I have also many reasons to acknowledge my dear family Dr. Silvia H. Santagneli, but the one I am must thankful is for her guidance during my undergrad, master and PhD, for teaching me since the start, points of experimental science and for encourage my career and have provided me a lot of opportunities.

My gratitude to the whole Photonics Materials Group, especcialy: Professor Dr. Marcelo Nalin, Prof. Sidney Ribeiro, Prof. Edson Pecoraro and Dr. Danilo Manzani and Ferminio Cesar Polachini; and to my labmates, Karina, Moliria and Rafael. Specially Karina for her friendship here and during my stay in Quebec.

Prof. Hellmet Eckert and Dr. Marcos de Oliveira Jr. from Universidade Estadual de Sao Paulo, for had been my collaborators, providing investigation of strucutural properties of FP glasses by NMR and EPR techniques.

Concerning my stay in Quebec, I would like to thank Younes students, Maxime, Mathieu Desjardin, Mathieu Chazot, Mathieu Boivin, Guillaume, Tea, Rim, Mathilde and Mohammed, who helped during my stay, and facilitate my day to day life in the lab.

Thanks also to Steeve Morrency for the help and learning with the fiber drawing process, which we spent a lot of afternoons until succeed. It would not be possible without his help.

Also Prof. Dr. Denis Boudreau and his students from Univerté Laval – Quebec – Canada, who were always kind to me and helped in my stay in Quebec.

I would like to express my appreciation to my family and childhood friends, especially to my mom Selma, daddy Laercio and my sister Gabriela, even with all its simplicity they

provided me the chance to get here. Also, my appreciation to Aline, for her support and advices to work even harder every time i though about giving up, especially when i was far from.

Finally, my acknowledgments to São Paulo State University - Araraquara – through Institute of Chemistry – that has held all my studies since the beginning of my undergrad in 2007. I am finishing a 10-year process, which definitely changed my perspectives. And to Capes, for the financial support in all Ph. D. steps.

.

1. INTRODUCTION

Glass is one of the oldest materials known from at least 7000 B.C. Its transparency ranging from the ultraviolet (UV) to the near-infrared (NIR) enables multiple applications in different fields like glazing, optics (e.g. lenses, objectives, etc.), telecommunication (e.g. optical fibers), astronomy (e.g. large mirrors for telescopes) (PHILLIPS, 1960). Among the numerous applications that rely on the emission, transport, conversion or detection of light (in the optical range of the electromagnetic spectrum), some of them involve a specific operation in the deep-ultraviolet (DUV, 200-300 nm) and vacuum-ultraviolet (VUV, 120-200 nm) regions. For instance, one can cite laser technologies for DUV microlithography equipment, microlithographic lens and photomask (EHRT; SEEBER, 1991; RAO, 2013), where fluoride crystals and vitreous silica are well-known materials traditionally used. There are also industrial and biomedical sensing applications, determination by atomic absorption spectroscopy (AAS) of chemical species that have atomic absorption in the deep-UV region as phosphorus and sulfur (DE CAMPOS et al., 2011).

Historically, UV grade silica glass has been used in the DUV and VUV down to 150 nm and for light transmission step-index silica fibers with high OH in the core and fluorine doped clad have been used down to 160 nm (SKUJA et al., 2003). However, they suffer from solarization effect caused by defects concentration increasing which leads to optical absorption in the deep-UV. As long-term stability of light transmission is highly desirable in optical systems designing, especially in high performance spectroscopy applications, the development of a new kind of DUV fibers is of major importance.

Fluoride glasses based on aluminum fluoride and other metal fluorides with wide band gap (LiF, MgF_2, AlF_3, CaF_2, BaF_2, NaF) have extended transmission in the UV with a cut-off wavelength around 160 nm, near to that of silica glass. However, their tendency to crystallize during glass manufacturing or fiber drawing strongly limits their fabrication in the form of optical fiber. Among the glass compositions and systems explored to date proposed an alternative to existing UV-transmitting optical materials, glasses based on mixed fluoride-phosphate systems appear as excellent candidates. In fluoride-phosphate glasses, the phosphate component generally improves the glass-forming ability and its glass stability

against crystallization, while the fluoride components provide some specific optical features (low-phonon energy, low refractive index, extended UV optical transmission).

A few works in the development of optical fibers based on fluoride-phosphate glasses transmitting deep-UV light have been reported in the literature, to the best of our knowledge. To date, only silica glass fiber, so-called UV-grade silica, is used for DUV optical transmission. So, in this thesis, we aim at developing and characterizing novel fluoride-phosphate glass optical fibers transmitting in the UV region.

1.1. MATERIALS WITH (LARGE AND) EXTENDED TRANSPARENCY IN THE UV

Optical materials with extended transparency in the DUV and VUV regions are of great importance for applications in high performance optics and laser technologies for medical application in angioplasty and perforation of heart muscle during bypass surgery (KHALILOV et al., 2015), microlithography equipment where deep-UV light is used to produce integrated feature sizes on a semiconductor computer chip where the resolution of the final circuits is inversely proportional to the wavelength of the laser used to photo-write the masks and special UV optics (VYDRA; SCHOETZ, 1999). Typical excimer lasers operation wavelengths are 351 nm (XeF), 308 nm (XeCl), 248 nm (KrF) and 193 nm (ArF) (RAO, 2013).

Another application is the determination of chemical species with absorption in the deep-UV region as phosphorus and sulfur that can be determined by direct AAS measurements since the primary resonance lines (most sensitive) are in the VUV at 177.5, 178.3 and 180.7 nm, respectively (DE CAMPOS et al., 2011) but is not typically determined because the VUV region is not adequate for commercial instruments since intense and stable light sources are not available (WELZ; SPERLING, 2008).

1.1.1. FLUORIDE CRYSTALS AND VITREOUS SILICA AS MATERIALS FOR UV OPTICS

Fluoride crystals, as CaF_2, LiF, MgF_2, BaF_2, BeF_2 and vitreous silica are well-known materials traditionally used for UV optics (LUCAS; SMEKTALA; ADAM, 2002). However, the production of fluoride single crystals is expensive, and not adapted for large scale manufacturing. On the other hand, glassy materials are easy to fabricate and to be obtained as optical fibers that can guide UV light and can be used for laser technologies and would facilitate the development of systems for remote sensing of chemical elements by AAS. Vitreous silica is produced in a form of multimode fibers with undoped core having high OH-content and fluorine doped cladding and is used in the UV region (OTO, 2007). Fluoride glasses are also characterised by a large transparency from the UV down to 160 nm to the infrared up to 7 μm (KITAMURA; HAYAKAWA; YAMASHITA, 1990). BeF_2 based glasses could be the best UV-transmitting glass down to 150 nm, but unfortunately, they are very toxic (WILLIAMS et al., 1981).

1.1.2. MIXED FLUORIDE-PHOSPHATE GLASSES

As an alternative to vitreous silica, fluoroaluminate glasses also presents higher transmission in the UV region. However, the lower viscosity value at the drawing temperature induces higher tendency to crystallisation. Since these advantages result primarily from the strong ionic character of fluoride glasses, considerable progress can be made by developing mixed fluoride-phosphate glasses (MÖNCKE et al., 2005).

Mixed fluoride-phosphate (FP) glasses are a compromise between the excellent phosphate properties such as high mechanical strength and glass-forming ability with fluoride properties as low refractive index, low partial dispersion, good laser properties and broad optical transmission windows ranging from ~160 nm to 4000 nm avoiding the corresponding drawbacks of each class of glass which lead in difficulties in fiber drawing.

Beyond the high transparency in the UV region and the possibility to achieve glasses with higher thermal-stability, an important parameter for drawing fibers, others important properties for photonics can be obtained by mixing fluoride and phosphate. Phosphate glasses

usually allow higher concentrations of rare earths dopants. But these glasses, present high phonon energy and OH^- species at a level that can introduce high losses to the RE's quantum efficiencies via non-radiative decay processes, contrary to fluoride glasses, with relatively low maximum phonon energy (~500 cm^{-1}), opening the possibility to design new-generation of UV lasers, optical amplifiers, radiation dosimetry (DE OLIVEIRA et al., 2015; KALNINS et al., 2013; WANG et al., 2015) and other photonic devices based in fibers.

Preliminary studies on fluoride-phosphate systems based in polyphosphates and fluorides have shown good combination of many desirable properties of the fluorides and phosphate components of the glass such as high transparency from UV to IR and low refractive index and are summarized in the Table 1.1 (EHRT, 2015).

Table 1.1. Properties of mixed fluoride-phosphate glasses; composition, glass transition temperature (Tg), refractive index (n) and UV edge (λ_0). Adapted from (EHRT, 2015).

Glass composition	Tg(^{0}C)	n	UV edge λ_0(nm)
$39AlF_3$-$23SrF_2$-$28CaF_2$-$10MgF_2$	400	1.405	150
$2Sr(PO_3)_2$-98(AlF_3, Mg/Sr/CaF_2)	410	1.420	153
$4Sr(PO_3)_2$-96(AlF_3, Mg/Sr/CaF_2)	440	1.435	155
$10Sr(PO_3)_2$-90(AlF_3, Mg/Sr/CaF_2)	445	1.460	160
$20Sr(PO_3)_2$-80(AlF_3, Mg/Sr/CaF_2)	490	1.504	165
$40Sr(PO_3)_2$-60(AlF_3, Mg/Sr/CaF_2)	500	1.506	178
$80Sr(PO_3)_2$-20(AlF_3, Mg/Sr/CaF_2)	540	1.580	-
$100Sr(PO_3)_2$	485	1.560	-
$10P_2O_5$-Al/YF_3, Mg/Sr/Ba/CaF_2,NaF	421	1.481	-

From the structural point of view, the short-range order of phosphate is usually described in terms of the $Q^{(n)}$ terminology, where n is the number of P next-nearest neighbors per P tetrahedron as shown schematically in Figure 1-1.

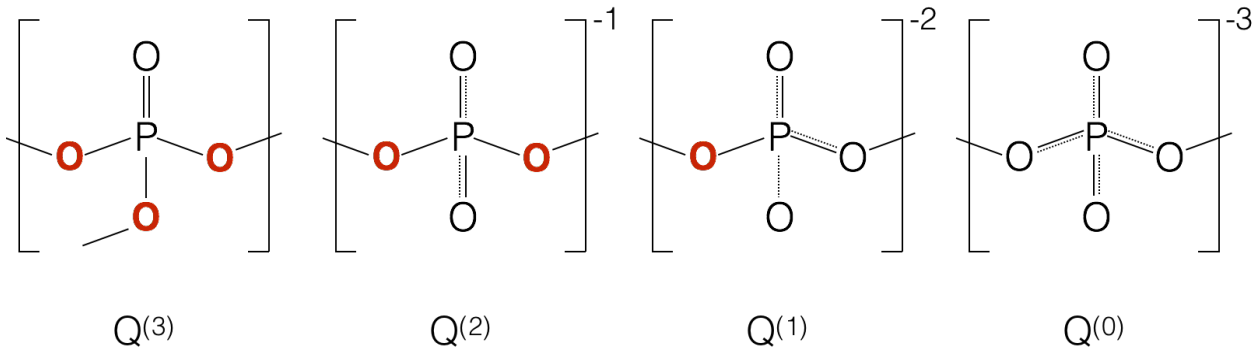

Figure 1-1. Schematic representation of Q^n phosphate tetrahedral units.

In fluoroaluminate glasses, AlF_6-octahedra connected by shared corners are proposed as the main glass forming entity (MÖNCKE et al., 2005). In the FP glasses, the structure consists of interconnected $Al(O/F)_6$-octahedra and PO_4-tetrahedra cross-linked by modifier cations, which the formation of P-O-Al linkages increases the rigidity of the structure, increasing the forming glass ability and slowing the nucleation process (DE OLIVEIRA et al., 2015). And when the efforts come to the development of highly UV transparent and RE-doped compositions, with excellent physical properties, the goal is to design a framework structure dominated by bridging oxygen links between the network formers, with the lowest amount of phosphate, resulting in high mechanical and thermal stability for fiber drawing, high UV optical transmission, while at the same time, creating a fluorine dominated low-phonon energy environment for the luminescent ions, which favours high fluorescence quantum efficiencies and long excited-state lifetime values.

In practice, manufacturing glasses with high UV transmission is difficult from a practical point of view. First, the UV absorption is dominated by electronic transitions from the valence to the conduction band. The bonds present in the structure dominate the energy gap between the valence and conduction bands, and thus the energy of the transition. The short-range structure dominates the electronic transitions (BERSUKER, 2010). In crystalline CaF_2 for example, the transition occurs at ~10 eV (124 nm) and for the SiO_2 glass, occurs at ~8.25 eV (150 nm), which is similar to that of fluoroaluminate glasses based on AlF_3 and MF_2 (M = alkaline earth metal). Their energies are comparable with those of fluoride single crystals, and the addition of phosphates decreases the band gap energy (Table 1.1).

Besides this fundamental intrinsic absorption, extrinsic absorptions caused by trace impurities restrict the practically achievable transmission. Transition metal (TM) ions as Fe^{3+}, Cr^{3+}, Cu^{2+}, are the main trace impurities present in the glass and their charge transfer bands have high absorption coefficients (EHRT, 2015). Even small amounts of TM ions (ppm range) may cause dramatic deterioration of the UV transmission and may also increase the material sensitivity to radiation damage. Charge transfer transitions $\varepsilon \geq 10^3$ $M^{-1}cm^{-1}$ are preferred over electron transitions bands with $\varepsilon = 10^{-2}$ to 10^2 $M^{-1}cm^{-1}$.

Iron is a particularly undesirable impurity which is easily introduced into the glass from the starting raw materials in small quantities (ppm) and the possible contamination from the melting technique and method of processing used (COOK; MADER, 1982). Two broad bands are observed in glasses due to Fe absorption at around 200 nm and 250 nm. The band at 250 nm is attributed to Fe^{3+} and the band at 200 nm to Fe^{2+}.

The effect of metallic impurities (Ce, Pt, Fe, Ni, Cr, Cu, Pb, Sn, Ti) in the ppm range on the UV absorption edge of fluoride-phosphate glasses were intensively investigated (EHRT, 1996; EHRT; LEISTER; MATTHAI, 2001; MATTHAI; EHRT; RÜSSEL, 1998), and Seeber at al. (EHRT, 2015) found that the UV absorption of the glass depends also on melting conditions, with variations in the observed UV absorbance intensity, when different atmospheres and container materials were used.

Glasses melted under reducing conditions (i.e. with added reducing agents or in carbon crucible) can exhibit much greater UV transmission near 250 nm than glasses melted under oxidizing conditions due to reduction from Fe^{3+} to Fe^{2+}. For small content of iron, 6 ppm, the effect is smaller (EHRT, 2015).

1.1.3. DEEP-UV FIBER AND RADIATION INDUCED DEFECTS

Another important property of optical materials is their resistance to radiation damage. Ionizing radiation produces free holes and electrons in glass which are then trapped, forming defect centers. These defects centers cause a decrease in optical transmittance in the UV and visible range of the spectrum and are commonly referred to solarization.

The silica fiber with high OH content core possesses high initial transmission, which is due to the smaller concentration of intrinsic defects, but when irradiated by UV light,

solarisation process are important and decreases considerably the UV transmission (OTO, 2007).

In FP glasses, the solarisation effect depends on iron content, melting conditions, radiation doses and heat treatment. The formation of color centers by excimer laser radiation is likely to be the result of photoionizable multivalent ions present as trace impurities, mainly iron, into the glass (JIANG et al., 2015).

Ehrt et al (EHRT et al., 1994) observed that fluoride-phosphate glasses with high iron content (27 ppm) melted in reducing conditions have a better UV-transmittance near 250 nm before irradiation since most of the iron exists in the Fe^{2+} state, but stronger solarisation effect was induced by excimer laser radiation than the same glass melted in oxidizing conditions. For low iron content (6 ppm), a weak susceptibility to solarisation was observed at low radiation density.

Unlike silica glass, FP glasses with low phosphate content possess less oxygen defects. Controlling the impurities in the glass can have greater resistance to radiation. Therefore, FP glass fibers with low content of impurities can be UV-transmitting optical materials that are complementary to silica glass fiber and fluoride crystals.

To achieve ultra-low losses in FP glass fibers, similar to those obtained sin silica fiber, which technology is pretty mature nowadays, it is not an easy task and few works in the literature report on fabrication on FP glass fibers. Step-index FP fiber were fabricated by Zou et al. drawing a preform in the system P_2O_5-AlF_3-YF_3-MgF_2-RF_2-NaF, (R = Mg, Ca, Sr and Ba) obtained by extrusion. The minimum loss they measured in the UV was 0.11 dB/m at 365 nm, while extrinsic absorption bands were observed due to the presence of transition metal impurities at 340 nm (Fe^{3+}), 520 nm (Cr^{3+}, Ni^{2+}) and 800 nm (Cu^{2+}, Fe^{2+}) (ZOU; ITOH; TORATANI, 1997; ZOU; TORATANI, 1997). Using a commercial fluoride-phosphate glass (N-FK51A), Kalnins et al. have prepared an unclad optical fiber by drawing preforms also produced by extrusion. Preform neck-down crystallization issues during fiber drawing were observed and they reported a minimum losses of 3.05 dB/m at 405 nm only after increasing the preform feed-rate and drawing speed, which decreased the time of exposure of the preform in the furnace and consequently, the surface crystallization issues (KALNINS et al., 2011). They also showed that treatment of extruded preforms prior to fiber drawing further improved optical fiber loss to 0.5-1 dB/m. Thus, in this thesis, there is an interest in the opportunities

offered by the high transparency in UV regions of mixed FP glasses for fabrication of optical fiber for technological applications.

1.2. STATE OF ART: GENERAL CONSIDERATION ON GLASSES

1.2.1. GLASS DEFINITION

In popular usage, "glass" denotes a transparent and fragile material and is often used to refer only to that based on the chemical compound silica (silicon dioxide), which is familiar from use as window glass and in glass bottles.

In scientific language, glass is a non-crystalline solid, isotropic material obtained by rapid cooling of a liquid. However, the fast cooling of liquid is not the only method for obtaining non-crystalline solids. Basically, non-crystalline solids can be obtained by fast cooling maintaining the structural disorder of the liquid phase, by mechanical compression, interrupting the order of a crystal and by evaporation, using the disorder nature of the gas phase (ZARZYCKI, 1982).

From a structural point of view, a non-crystalline solid is characterized by the absence of long-range order which defines crystalline materials and as in the amorphous solids, the atomic structure of glass lacks any long-range translational periodicity (GUPTA, 1996).

In a good glass former, the network structure is topologically disordered, because these structures possess intrinsic resistance towards crystallization, which requires topological changes (bond breakage and reformation) and the short-range order is the same as in the corresponding crystal. For example, the SiO_4 tetrahedra that form the fundamental structural units in silica glass represent a high degree of order, i.e. every silicon atom is coordinated by 4 oxygen atoms and the nearest neighbour Si-O bond length exhibits only a narrow distribution throughout the structure (GUPTA, 1996).

Not all non-crystalline solids are glasses. They can be classified as amorphous solids or glasses. The non-crystalline solid is a glass, if its short-range order is the same as that in its molten state. This condition is clearly satisfied for glasses formed by cooling a molten liquid because the structure of a melt is frozen during the transition from liquid to glass. Whether a non-crystalline solid is made by melt-cooling or by other methods (for example, evaporation) it is called glass as long as it satisfies this condition. If these conditions are

respected, but short-range order of the glass is different from the molten liquid the material will be classified as an amorphous solid. In addition, amorphous solids and glasses are distinct thermodynamically. The free energy of amorphous solids is less than that of super-cooled liquid and they do not show structural relaxation. The heating of these substances leads to rapid crystallization or decomposition of structure before their melting point is reached. Contrariwise, the glass passes progressively from a solid state to a liquid state with the successive increase of temperature. Such transition (from solid to molten state or the reverse one) is called "glass transition". So, one of the most used and cited in the literature definition of glass have been proposed by Zarzycki (ZARZYCKI, 1982): "Glass is a non-crystalline solid exhibiting the phenomenon of glass transition temperature."

1.2.2. GLASS TRANSITION TEMPERATURE (TG)

The conventional method for producing a glass is the very rapid cooling of the liquid, in order to prevent crystallization. Decreasing the temperature, an increase in viscosity of the liquid rapidly occurs, leading to the freezing of the liquid to the final solidification. Temperature decreases leads to a volume variation (contraction of the substance) and when the solidification point is reached, two distinct phenomena can occurs (Figure 1-2).

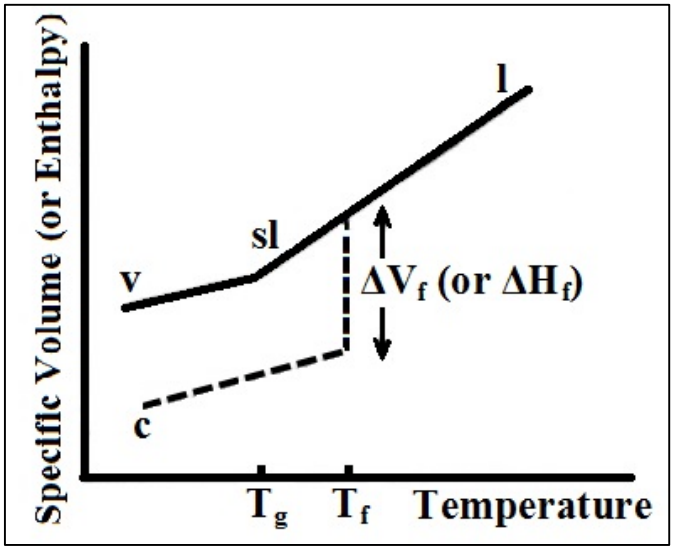

Figure 1-2. Variation of the specific volume with temperature. Adapted from (ZARZYCKI, 1982). (l – liquid; sl – super-cooled liquid; c – crystal; v - glass

(i) The liquid crystallizes and a discontinuity of ΔV_f is introduced. This discontinuity is characteristic of a first order transition.

(ii) Crystallization is prevented and the liquid passes to the super-cooled state starting from certain temperature and there is no discontinuity in the specific volume versus temperature curve shown below in proximity of the transition. The jump in the curve shows the transition from the supercooled state to the glassy state. The glass transition temperature, Tg, is defined as the point where a change in slope takes place. This is associated with a change in the thermal expansion coefficient from the glass to the liquid state. This type of transition which does not involve any discontinuity in the V-T curve (and similarly in the enthalpy versus T curve) is often called a second order transition.

1.2.3. GLASS OPTICAL PROPERTIES

Light transmission, absorption, reflection, and scattering describe the macroscopic aspects of light-glass interaction. These optical properties can be simply characterized by the spectral transmittance as a function of wavelength of the irradiating light, and depend on the elements of which it is composed, including the nature of its anions and cations.

Spectral transmittance is the ratio of the incident light leaving the glass to the light of monochromatic light radiation.

The incident light can be divided over the total interactions:

$$I = I_r + I_{abs} + I_t + I_{sc} \quad (1)$$

where I_t is the transmitted light, I_{abs} the absorbed light, I_r the reflected light and I_{sc} the scattered light. Therefore, light is part absorbed, reflected and transmitted.

Absorption in glass is characterized by a decrease in transmitted light intensity through the sample that is not accounted for by reflection losses at the surface or scattering by inclusions. The quantity used to discuss absorption as a function of wavelength in glass is the transmittance (T), which is the ratio of the transmitted light intensity (I) to the initial light intensity (I_0) after passing through a glass plate of thickness l:

$$T = \frac{I}{I_0} \quad (2)$$

The transmittance can be expressed to the more common percent transmittance (%T) through:

$$\%T = 100T \tag{3}$$

Sometimes it is more practical to look at the optical spectra in terms of absorbance rather than the transmittance. Absorbance (A) is defined as the $\log_{10}$ of (1/T):

$$A = log_{10}\frac{I_0}{I} = log_{10}\frac{1}{T} = 2 - log_{10}\%T, \tag{4}$$

$$\%T = \frac{100}{10^A} \tag{5}$$

When the absorbance changes linearly with concentration of the absorbing species (C), then Beer's law, which relates absorbance with concentration, path length (l) and extinction coefficient (ε), is applicable

$$A = \varepsilon Cl \tag{6}$$

The typical units of ε are liters mole^{-1} cm^{-1} and are often omitted. From Beer's law we see that the absorbance changes with path length which light is passing through. Because of this, the spectra (in A or %T) must list the sample thickness. Therefore, absorbance can also be normalized to path length in terms of an absorption coefficient (α) (cm^{-1}).

1.2.4. REFLECTION

The total transmission of a glass is determined by reflection at the glass surfaces and optical absorption in the glass. Neglecting multiple reflections between the glass surfaces, the total transmission in air of a flat sample at a specific wavelength is approximately equal to $(1\text{-}R)^2e^{-\alpha l}$ where α is the absorption coefficient, l the thickness of the glass, and R the air–glass reflection coefficient. Reflectance depends strongly on the quality of the glass surface, the angle of incidence, the indices of refraction of the glass and the surrounding medium, and the wavelength. Reflectance can be specular, as in polished or precision-molded surfaces, or diffuse for ground or irregularly etched ones. The fraction of light of normal incidence reflected by a single plane surface is given by: $R = [(n\text{-}1)/(n+1)]^2$, in which *n* is the refractive index of the glass at the wavelength of interest (the refractive index of air is assumed to be 1).

1.2.5. REFRACTIVE INDEX

The refractive index, denoted by n, is a dimensionless quantity characteristic of a medium. It depends on the measurement wavelength but also on the characteristics of the environment in which light propagates. In order to understand the propagation of light in a glass and thus the refractive index, we are interested in a simple system with two homogeneous isotropic media of respective refractive indices n_1 and n_2, as shown in Figure 1-3, Where we assume that $n_1 > n_2$. We consider an incident light beam making an angle θ_1 with the normal to the tangential plane to the boundary surface between the two media. This ray is reflected and refracted if the angle of incidence is different to zero.

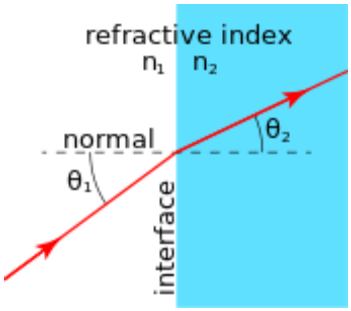

Figure 1-3. Refraction of light phenomenon in the passage through two homogeneous isotropic media of respective refractive indices n_1 and n_2. Adapted from (Bach et al., 1998)

The Snell-Descartes law specifies that: the reflected and refracted ray are in the plane defined by the radius incident and normal to the surface; the angle of reflection is equal to the angle of incidence; The relationship between the angle of refraction and the angle of incidence is $n_1 \sin\theta_1 = n_2 \sin\theta_2$

Refraction is the scientific term that applies to the deflection of light due to the variation of the refractive index. There is refraction as long as $\sin\theta_1 < \sin\theta_2 = n_2/n_1$, as long as $\theta_1 < \theta_2 = \arcsin(n_2/n_1)$, where θ is the critical angle.

When $\theta_1 > \theta_2$: there is total reflection.

1.2.6. TRANSMISSION WINDOW

Glasses can be transparent from the UV to the IR regions depending on the composition. The region of transparency is known as transmission window and is limited intrinsically by three physical phenomena: electronic absorption at short wavelengths (UV-Vis range), multiphonon absorption at long wavelengths (IR range), and scattering in between. Extrinsic losses are often observed within this window and arise from impurities in the glass. Glasses possess a characteristic energy gap, Eg. Incident photons with energy exceeding this gap, hv>Eg, will excite an electron from the valence to the conduction band creating an electron-hole pair. Thus occurs in multiple non-radiative steps generating phonons rather than photons. The electronic band gap depends on the electronic configuration and positional arrangement of the atoms in the material. In crystalline materials, the lattice positioning dictates a long-range atomic order suggesting a sharply defined band gap and steep rise in absorption at short wavelengths. However, disorder due to crystal defects, and more importantly temperature, ensures the band gap is not sharply defined and shifts the electronic edge absorption to longer wavelengths and imparts a more gradual dependence of absorption on wavelengths, resulting in the called Urbach tail (BACH; NEUROTH, 1998). In the amorphous form of the same material, the crystalline short-range atomic order is typically retained, but the long-range positioning does not keep to any crystal lattice. The electronic absorption edge therefore is usually situated in approximately the same energy (wavelength range) as for the crystalline form, but is less sharply defined and takes on a more gradual wavelength dependence.

The IR cutoff is determined by the multiphonon absorption edge and is governed by vibrational resonances of the atomic network which depend on atomic mass and bond strength. For glasses with larger atoms and weaker bonds, this vibrational resonance occurs at lower frequencies, pushing the fundamental absorption infrared cutoff to longer wavelengths (BRINKMANN et al., 2007).

The wavelength of absorption of a bond is expressed by:

$$\lambda = 2\pi c\sqrt{\frac{\mu}{\kappa}} \tag{7}$$

where, c is the speed of light in vacuum, μ the reduced mass and κ the molecular force constant. The most common extrinsic absorption centers in the IR are OH, CO_2 and iron. The multiphonon edge is shifted to longer wavelengths (smaller frequencies) by heavier ions (greater M) and weaker bonds (smaller f), which is why chalcogenide glasses transmit further into the IR than more traditional oxide glasses.

Figure 1-4 shows the transmission window for 3 different type of glasses, oxide, fluoride and chalcogenide.

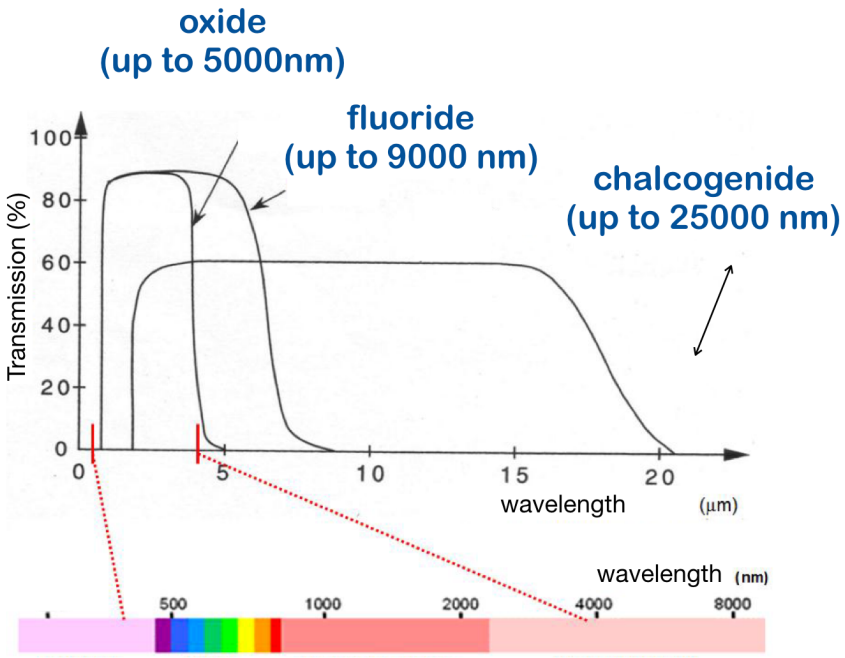

Figure 1-4. Example of transmission window for different classes of glass adapted from (NALIN et al., 2016).

1.3. FUNDAMENTAL ASPECTS OF OPTICAL FIBERS

1.3.1. PROPAGATION IN A CONVENTIONAL STEP-INDEX FIBER

Conventional optical fibers are cylindrical waveguides made of glass and composed of an inner part, the core, with refractive index n_{core}, surrounded by a glass cladding with slightly lower refractive index $n_{cladding}$, $n_{cladding} < n_{core}$. This structure is eventually covered

with a polymeric coating for mechanical protection and protection against degradation of the material by the environment, as schematized in Figure 1-5.

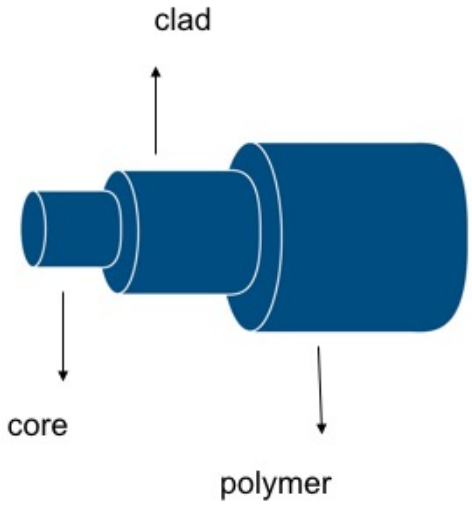

Figure 1-5. Schematic figure of a conventional optical fiber.

The light is totally reflected at the interface by total internal reflection if the angle of incidence is greater than a critical angle (θ_c). This property allows guiding light into the core of step-index optical fibers.

The total internal reflection condition at the interface between the core and the clad is limited by a maximum angle of incidence at the interface of the core to the external medium:

$$\theta_{max} = arcsin\sqrt{{n_{core}}^2 - {n_{cladding}}^2} \quad (8)$$

where n_{core}, n_{cladding} are the core and cladding refractive index, respectively.

This angle determines the cone of acceptance of the fiber, and the sine of this angle is called the numerical aperture (NA), which is used to characterize the amount of light that the fiber can guide through the core:

$$\text{NA} = \frac{\sqrt{{n_{core}}^2 - {n_{clad}}^2}}{n_0} \quad (9)$$

The higher the NA, higher the angle of acceptance. Thus, the larger the NA of the fiber, the greater will be the ability to guide light into the core, which is defined by the ratio:

$$\Delta = \frac{\sqrt{{n_{core}}^2 - {n_{clad}}^2}}{n_0} = \frac{NA^2}{2{n_{core}}^2} \quad (10)$$

In most optical fibers, the core and cladding refractive index are not too different. When $\Delta < 0.01$, the fiber is considered single-mode.

1.3.2. MODES OF PROPAGATION

Depending on the relative diameter of the fiber core to the total fiber, light can travel through one or more paths, such paths are called modes. Conventional fibers can be of three types: multi-mode - step-index fibers, multi-mode - graded-index fiber, and single-mode – step index fiber fibers. The step-index fibers exhibit a discontinuity of the refractive index at the core-cladding interface, while the graded-index fibers exhibit a continuous variation of the refractive index in the direction from the core to the shell. The single-mode fibers are generally of step index and have a small core diameter. Figure 1-6 shows the three types of fibers.

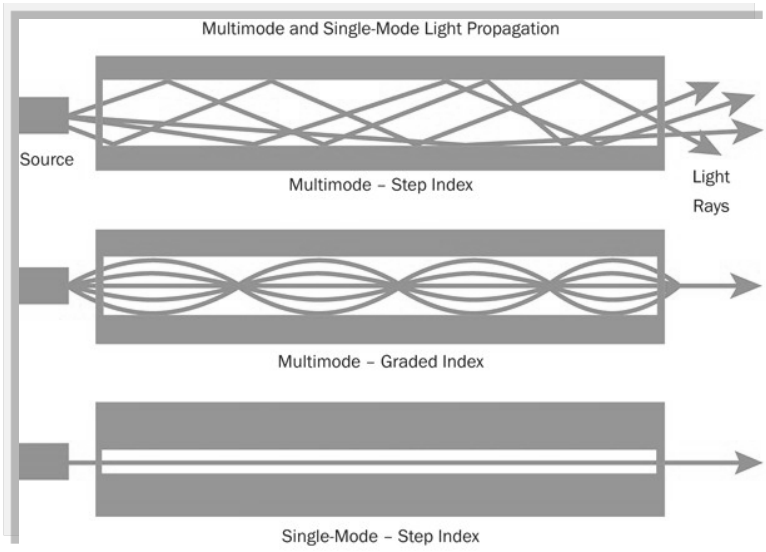

Figure 1-6. Schematic of light-ray propagation in multimode step-index, graded-index (b) and single-mode optical fiber. Adapeted from fiber optic share website (www.fiberopticshare.com)

1.3.3. OPTICAL LOSSES IN THE FIBER

Efficient light transmission at the operational wavelength(s) is the primary function of optical fibers needed for a range of applications (e.g. long-haul telecommunications, fiber lasers, optical delivery applications). Intensity loss, as light travels within the fiber is called "attenuation". To understand the attenuation mechanisms and the potential for their minimization is, thus, of great importance.

Any process that results in a reduction in the light intensity after propagation through a material contributes to the observed optical attenuation. In principle, all attenuation mechanisms can be followed back to the multilength scale structure of the glass itself, as atomic structure and point defects or structures arising from the fiber fabrication process, as interfacial structure at the core-cladding interface and uniformity of core-cladding structure along fiber length. Thus, the control of material structure through material processing, composition and fiber fabrication is the main way to reduce losses in the final optical fiber.

The global transmission of an optical fiber can be measured in terms of the input and output optical power, P_0 and P_L, respectively, observed after light propagates a distance l through the fiber length:

$$P_L = P_0 e^{-\alpha_{total} l} \tag{11}$$

where α_{total} is the total attenuation coefficient (involving all contributions). Transmitted power decreases exponentially with propagation distance (z) through the fiber, due to the losses.

The total attenuation coefficient above is often expressed in dB/Km unit:

$$\alpha_{total}\left(\frac{dB}{Km}\right) = \frac{10}{z}\log\left[\frac{P_0}{P_L}\right] = 4.343\alpha(Km^{-1}) \tag{12}$$

This final parameter is often referred to as the "optical fiber loss".

It is important to note that multiple contributions to a global transmission value arise from intrinsic fiber material properties as well as extrinsic attenuation mechanisms associated with fiber fabrication (preform development, drawing conditions). Therefore, the total attenuation can be divided into intrinsic and extrinsic source of losses. Each of these can be further subdivided into absorption loss and scattering loss.

1.3.3.1. INTRINSIC OPTICAL ABSORPTION

The intrinsic optical absorption responses of core and clad glasses used were previously discussed as the primary factor dictating the transmission window in Item 1.2.6. (and ultimately the operational wavelengths) for an optical fiber. It is delimited on the long-wavelength side by absorption from multiphonon (vibrational absorptions of the chemical bonds and their harmonics) and on the short-wavelength side by the band-gap (absorptions of light through transitions of the valence band for the conduction band of the material).

Intrinsic light scattering arises from *Rayleigh scattering*, which is caused from micro-fluctuations in the refractive-index of the material, caused by changes in density and composition. The degree of scattering depends on the size of the scattering centers and the wavelength of the radiation, and the scattered intensity depends inversely on the fourth power of the wavelength:$I \propto \frac{1}{\lambda^4}$.

1.3.3.2. EXTRINSIC OPTICAL ABSORPTION

In addition to this energy structure of the base glass that defines the transmission window, the presence of defects in the glass structure, fiber fabrication process and the presence of impurities can produce absorption in both frontiers of electromagnetic spectrum that limits the transmission window. When such absorption is localized at frequencies within the transmission window and/or at the operational wavelength of the fiber, such structural elements present a significant loss in the optical fiber systems.

Impurities, in their bonding with the primary material anion, can also give rise to impurity-driven vibrational modes which can absorb either at the fundamental or overtones frequencies. The most problematic impurities in the 1 to 10 μm range are light atoms and, in particular, hydrogen. Vibrational impurities are important not only as dissolved species but also as macroscopic heterogeneities and as surface impurities.

Similarly, impurities with metal-ion species, e.g. transitions metals, in the precursors reagents, inclusion during preform fabrication and/or drawing can also produce marked

attenuation in the UV-visible and near-IR spectral ranges. The most problematic impurities in the UV region, and very important for the scope of this thesis are TM, as mainly Fe, Cr, Co, even at small quantities in the ppm range. Such impurities come from the precursor reagents and also during the synthesis of the material.

Extrinsic light scattering arises from Mie scattering and imperfection such as bubbles, microcrystals and core-cladding boundary fluctuations. These defects arise during fiber fabrication and are responsible for the largest extrinsic losses that are sometimes observed.

1.3.4. PREDICTION OF LOSS MINIMA

The theoretical loss minimum α_{min} of an optical material as a function of λ can be determined by assessing the intrinsic attenuation process that defines the transmission window. These are usually assumed to be the multiphonon edge, the Rayleigh scattering and the electronic transition edge. The schematic of such an "intrinsic window", known as a V-plot, is shown in Figure 1-7.

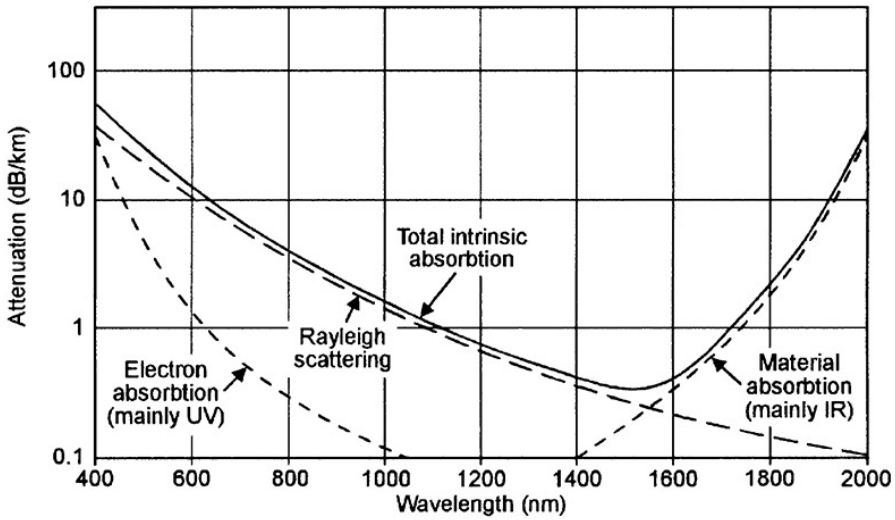

Figure 1-7. V-curve due to intrinsic optical absorption high grade silica fiber. Adapted from (MIMURA; NAKAI, 1991)

1.4. FUNDAMENTAL ASPECTS OF SOLID-STATE NMR.

Nuclear Magnetic Resonance Spectroscopy (NMR) is based on the magnetic properties of atomic nucleus. This magnetism reflects their spin angular momentum, represented by the vector opearator I. Nuclear spins are subject to orientational quantization, according to $\mu_z = m\hbar$, with energetically degenerate characterized by the quantum number $m \in \{I, I-1, I-2, \ldots -I\}$, where I is the nuclear spin quantum number. Each nuclear magnetic moment (μ) is related to the nuclear spin I of the nucleus and given by

$$\vec{\mu} = \gamma\hbar\vec{I}$$

where γ is the magnetogyric ratio, and h is the Planck's constant.

In the presence of an external magnetic field B_0 the magnetic moment interacts with this field, with energy

$$E = -\vec{\mu}\overrightarrow{B_0}$$

1.4.1. THE BASIC INTERACTIONS IN SOLID-STATE NMR.

1.4.1.1. THE ZEEMAN EFFECT

The Zeeman effect reults from an external perturbationof the spin system. Application of an external magnetic field $\underline{B}^0$ annihilates the isotropy of space. The formerly degenerate energy levels split into (2I + 1) levels of energy.

$$E_m = -m\gamma\hbar B^0$$

where I represents the spin number os the nucleus, m = (I, I-1, …, -I) the magnetic quantum number, γ its gyromagnetic ratio, and h is Planck's constant. The difference ΔE of two neighboring levels due to the Zeeman effect is directly field dependent. It is given by

$$\Delta E = \gamma\hbar B^0$$

and determines the resonance frequency of a nucleus for a given field strength. Hence, it is one of the parameters that influence the sensitivity of a nucleus.

Owing to its magnitude, the nuclear Zeeman Interaction is in general treated as the main interaction in solid state NMR. Thus, other nuclear interactions are considered as pertubations of the Zeeman interaction.

1.4.1.2. CHEMICAL SHIELDING – CHEMICAL SHIFT INTERACTION

Each nucleus is "chemical shielded" by a cloud of electrons. The external magnetic field $\underline{B^0}$ induces rings currents in the electron clouds at the differrents crystallographic sites. These circulating currents, in turn, generate and induce magnetic field $\underline{B}^{ind}$.

$$B^{ind} = -\sigma B^0$$

where σ is the magnetic shielding constant of the nucleus. $\underline{B}^{ind}$ is directly dependent on the external static field $\underline{B^0}$ and tend to oppose to the latter.

In solid state NMR, the chemical shielding is orientation dependent and can reveal information about the close surroundings of the nucleus. The chemical shielding is represented by a tensor (ellipsoid). The deviation of the tensor ellipsoid from spherical symmetry is an intuitive measure for the anisotropy of the chemical shielding. The isotropic chemical shielding is the average value of the three tensor components.

$$\sigma_{iso} = \frac{1}{3}(\sigma_{xx} + \sigma_{yy} + \sigma_{zz})$$

The chemical shielding anisotropy Δ_{cs} is defined as

$$\Delta_{cs} = \sigma_{zz} - \sigma_{iso}$$

The asymmetry of the chemical shielding is defined as

$$\eta = \frac{\sigma_{xx} - \sigma_{yy}}{\Delta_{cs}}$$

The effective field $\underline{B}^{eff}$ at the site of the nucleus is the sum of the external field $\underline{B}^{0}$ and the induced field $\underline{B}^{ind}$

$\underline{B}^{ind}$ is in the order of 10^{-4} of the static external field $\underline{B}^{0}$. However, $\underline{B}^{eff}$ is the characteristic for a given crystallographic site, resulting in a slightly shifted resonance frequency.

$$v^{eff} = v^{0}(1 - \sigma)$$

By introducing the definition of the chemical shift δ

$$\delta = \frac{v^{eff} - v^{ref}}{v^{ref}} * 10^{6}$$

The $\underline{B}^{0}$ dependence of the resonance shift is removed. Additionally, the originally small effect of the chemical shielding is multiplied by a factor 10^{6}. δ is defined in units of part per million (ppm), v^{ref} is the resonance frequency of the nucleus in a reference compound. Resonance that tend towards negative values of the δ (ppm) scale are termed shielded or shifted upfield. Resonances that tend towards positive chemical shift values (ppm) are termed deshielded shifted downfield.

1.4.1.3. DIPOLAR COUPLING

Due to its dipolar magnetic moment, each nuclear spin I generates a magnetic field surrounding it. Neighboring nuclear spins interact with this nuclear field directly trhough space. Each spin I is the source of a magnetic field and, in turn, experiences those generated by neighboring spins S. in the case of homonuclear dipolar coupling the spins I and S are of the same species. In the case of heteronuclar dipolar coupling the spins I and S are different.

The dipolar interaction can be described by substituting the quantum mechanical magnetic moment operator into the classical expression for the interaction between two point magnetic dipoles

$$\widehat{H} = -\frac{\mu_0}{4\pi}\gamma_I\gamma_S\hbar\left\{\frac{I \cdot S}{r^3} - 3\frac{(I \cdot r)(S \cdot r)}{r^5}\right\}$$

where I and S are the spin magnetic moments with their respective gyromagnetic ratios γ_I and γ_S, h is Planck´s contant and μ_0 is the permittivity of the vacuum. *r* is the internuclear distance between I and S.

The description of dipolar coupling illustrates best that the strength of the dipolar interaction between two nuclei depends in first approximation on the inverse of the cubic distance between them, that is $\widehat{H} \propto \frac{1}{r^3}$.

Dipolar coupling does not have any isotropic contribution. Its orientation dependence is of the form

$$(3cos^2\theta - 1)$$

and hence its averages to zero under magic angle spnning.

Since the sipolar interaction between two nuclei depends in first approximation on t he inverses of the cubic distance between them, it can be exploited to probe spatial proximities between nuclei. Therefore, the dipolar interaction can be *reintroduced* by sequences like REDOR or REAPDOR.

1.4.1.4. SCALAR COUPLING (J-COUPLIN)

Nuclear spins interact with each olther via the bonding electrons they share. The terms scalar coupling or J-coupling are frequently used for this indirect coupling. The participation of the bonding electrons gives rises to an orientation dependence that is different from the one of dipolar coupling. As a result, there exists an isotropic component that contributes to scalar coupling and persists even under magic angle spiining conditions in solids or Brownian motion in liquids.

1.4.1.5. ELETRIC QUADRUPOLAR COUPLING

All nuclei with a spin I>1/2 has a non-spherical charge distribution that gives rise to a nuclear electric quadrupole moment that interacts with the electric field gradient at the site of the nucleus.

Quadrupolar coupling is not completely removed by MAS. A second-order term persists, giving in many cases rise to characteristically broades resonances that can be characterized by the quadrupolar coupling constant *Cq* and the asymmetry parameter η_q.

In practice, *Cq* indicates the strength of the quadrupolar coupling between the nucleus and the electric field gradient of its proximate surroundings. It determines the linewidth of the NMR signal in the MAS dimension.

1.4.2. METHODS OF NMR SPECTROSCOPY

1.4.2.1. MAGIC ANGLE SPINNING

Powder samples consist of many crystallites with random orientations, their high number giving rise to a large distribution of spectral frequencies. Broad powder patterns are obtained, if the spectrum is recorded under static conditions. As a result, different crystallographic sites can overlap, concealing information. As mentioned above, this loss of spectral resolution can be eliminated in great part by magic angles spinning (ANDREW; BRADBURY; EADES, 1959).

The basic principle of MAS is that most of the nuclear spin interactions present an orientation dependence of the following form:

$$(3cos^2\theta - 1)$$

where θ is the angle between the static field $\underline{B^0}$ and the principal z-axis of the tensor ellipsoid of the nuclear spin interaction (FIGURE 1-8)

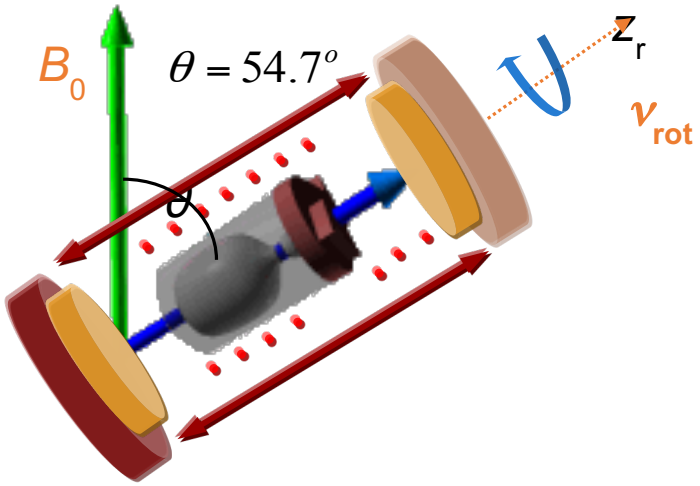

Figure 1-8. The magic angle orientation of 54.7°relative to the direction of the static field (B_0).

The aim os MAS is to average this term to zero. It takes advantage from the fact that the average of the nuclear orientation dependence under spinning can be shown to be

$$\langle 3cos^2\theta - 1\rangle = \frac{1}{2}(3cos^2\theta_r - 1)(3cos^2\beta - 1)$$

where θ_r is the angle between the spinning axis and the static field $\underline{B^0}$ and β is the angle between the apinning axis and the principal z-axis of the tensor ellipsoid of the nuclear spin interaction. If θ_r is set to be 54.74°, the magic angle, the term $\langle 3cos^2\theta - 1\rangle$ is zero under MAS conditions (Figure 25).

At present, MAS is the most commom technique to average out firs-order anisotropic interactions in powder samples. Second-order anisotropic interactions are not completely averaged to zero.

1.4.2.2. STATIC DIPOLAR NMR SPECTROSCOPY

Magnetic dipole-dipole couplings between and those in their vicinity result in a modification of the measured precession frequencies. The effect is distance dependent and anisotropic, depending on the interaction of the internuclear distance vector relative to $\underline{B}^0$, contributing to the NMR line-broadening effects observed in powered samples. There are homonuclear and heteronuclear contributions.

By systems characterized by the average mean square of the local field (the secon moment), which can be related to internuclear distance contributions by the van Vleck formulae (VAN VLECK, 1948).

$$M_{2,homo} = \frac{3}{5}(\frac{\mu_0}{4\pi})^2 I(I+1)\gamma^4\hbar^2 \sum_{i\neq j} r_{ij}^{-6},$$

$$M_{2,homo} = \frac{4}{15}(\frac{\mu_0}{4\pi})^2 S(S+1)\gamma_I^2\gamma_S^2\hbar^2 \sum_{S} r_{ij}^{-6}$$

Thus homo- or heteronuclear dipolar second moments represent quantitative criteria against which structural models can be tested in a rigorous fashion. In the following sections, various experimentaltechniques for obtaining such dipolar second moments are described and their significance for the structural analysis of glasses is highlighted.

1.4.2.3. ROTATIONAL ECHO DOUBLE RESONANCE - REDOR

Rotational echo double resonance (REDOR), a powerful experiment is able to provide site-selective dipolar coupling information under the high-resolution conditions afforded by magic angle spinning (GULLION, 1995). In general, the dipolar coupling constant oscillates according to the term sin $\omega_r t$ and is averaged out over the rotor cycle. However if we invert the sign of the dipolar Hamiltonian by applying a π-pulse to the nonobserved I spins somewhere during the rotor cycle, this average is nonzero; the interaction is recoupled and now interferes with the ability of MAS to provide signal refocusing.

Recoupling is accomplished by 180° pulse trains applied to the I spins, while the S spin signal is detected by a rotor-synchronized Hahn spin echo sequence. One measures the normalized difference signal $\Delta S/S_0 = (S_0 - S)/S_0$ in the absence (intensity S0) and presence

(intensity S) of the recoupling pulses. A REDOR curve is then generated by plotting $\Delta S/S_0$ as a function of the dipolar evolution time NTr, i.e., the duration of one rotor period multiplied by the number of rotor cycles. In the limit $\Delta S/S_0 < 0.2$ of short dipolar evolution times, the REDOR curves is found to be geometry independent and can be approximated by

$$\frac{\Delta S}{S_0} = \frac{S_0 - S}{S_0} = \frac{4}{3\pi^2}(NTr)^2 M_2$$

where the average van Vleck second moment can be extracted from a simple parabolic fit to the experimental data.

6. GENERAL CONCLUSION

The main goal of this Ph. D. research was to exploit the fluoride-phosphate properties in order to fabricate highly transparent optical fibers in the deep-ultraviolet and also to explore the structural and optical properties of the FP glasses for photonic applications.

Initially, FP glasses in the system 10 mol % $Ba(PO_3)_2$ and 90 mol % (AlF_3-CaF_2-SrF_2-MgF_2) have been prepared and showed to be suitable for fiber drawing thank to their excellent thermal stability against crystallization (> 100 ◦C). They also showed excellent optical transmittance when prepared from high-purity eagents, being transparent down to 180 nm in the DUV (75% for a 2 mm bulk sample). Core-cladding preforms where then produced by a modified build-in casting technique, preparing, separately, a tube for the clad, substituting the barium phosphate by strontium phosphate to decrease the refractive index and guarantee the guiding in the fiber by total internal reflection, and a rod for the core. Then the rod was inserted manually inside the tube and the fiber was then successfully fabricated from the as-prepared preforms through a fused silica crucible assembly. This alternative has shown to be suitable to overcome the superficial crystallization issues obtained during the preform method trials. An optical attenuation of 63 dB/m and 20-42 dB/m was measured on the produced step-index fibers at 244 nm and in the range 407-1750 nm, respectively. For the single-index fiber, the optical losses in the range 407-1750 nm are 0.7-5 dB/m. It is worth to mention that FP glass fibers fabricated by the crucible method were reported for the first time in the literature and constitutes a new route to address the challenges behind the complex fabrication of FP glass fibers and other glasses that suffer from superficial crystallization issues.

In the following step of the Ph. D. research, we have investigated the structural properties of a series of FP glasses with different F/P ratio to understand the structural evolution of these glasses, the origin of their thermal stability for fiber drawing and we also doped the glasses with RE ions to do a correlation between the structural and luminescence properties, important for photonic applications. We were able to provide a quantitative insight into the network organization by Raman and NMR techniques, and also the rare-earth coordination in these glasses as a function of the F/P ratio. The data suggest that as we decrease the F/P ratio, the network structure of these glasses is dominated by the formation

of Al-O-P linkages, which could also be quantified and the contribution of different $Q^{(n)}$ units. The glasses with higher F/P ratio are dominated by $Q^{(0)}$ species and the near-absence of P-O-P connectivity. As we decrease the F/P ratio both $Q^{(1)}$ and $Q^{(2)}$ units are present and dominant. The fluoride ions are found in a mixed Al/Ca/Sr/Mg environment and the local environment of the RE ions is characterized by a mixed fluoride/phosphate ligation, being quantified by EPR and optical spectroscopy. Some P-RE ligation remains even at the highest fluoride content in these glasses. The origin of their thermal stability, making these glasses suitable for fiber drawing, comes to the fact that this increase in connectivity by means of P-O-Al and P-O-P linkages, increases their thermal stability against crystallization, important for fiber drawing. Their high transparency in the DUV, comes from the high content of fluoride ions in a mixed alkaline earth environment, known to be highly transparent in this region due to their wide bandgap.

Finally, regarding the excellent luminescent properties found for the FP glasses with low phosphate content, we have prepared highly-pure fluoride-phosphate glasses co-doped with Gd^{3+}-Tm^{3+}-Yb^{3+}. First, using scandium as a diamagnetic mimic for the luminescent rare-earth species (Tm^{3+} and Yb^{3+}) with similar ionic radius, the ligand distribution surrounding the rare-earth ions has been quantified by $^{45}Sc/^{31}P$ rotational echo double resonance technique together with structural insights by means of other NMR techniques. The rare-earth ions have been found in a mixed fluoride/phosphate environment with a dominant fluoride ligation for these glasses and high F content. Second we have show upconverted emissions in UV region under 980 nm excitation from Tm^{3+} and Gd^{3+} ions for these glasses. The energy transfer mechanism between Gd^{3+}, Tm^{3+} and Yb^{3+} ions have been also proposed and suggests that UV emissions in 362, 310 and 290 nm may come from a five-photon, four-photon and three-photon energy transfer upconversion process, respectively. Emission of Gd^{3+} ion upon 980 nm excitation was observed for the first time in glasses. Highest average number of F atoms coordinate to rare-earth atoms are correlated with a more intense Gd^{3+} emission. The high transparency of these glasses also contributed to the high intense UV emissions observed.

REFERENCES

ANDREW, E. R.; BRADBURY, A.; EADES, R. G. Removal of Dipolar Broadening of Nuclear Magnetic Resonance Spectra of Solids by Specimen Rotation. **Nature**, v. 183, p. 1802–1803, 1959.

BACH, H.; NEUROTH, N. **The properties of optical glass**. 2nd ed. Berlin: Springer, 1998. 414 p.

BERSUKER, I. B. Electronic structure and chemical bonding. In: **Electronic structure and properties of transition metal compounds**. Hoboken: John Wiley & Sons, 2010. Chap. 6, p. 238-323.

BRINKMANN, M. Optical materials and their properties. In: TRÄGER, F. (Ed.). **Springer handbook of lasers and optics**. New York: Springer, 2007. p. 249-372.

COOK, L.; MADER, K. H. Ultraviolet transmission characteristics of a fluorophosphate laser glass. **Journal of the American Ceramic Society**, v. 65, n. 12, p. 597-601, 1982.

CAMPOS, R. C. de; CORREIA, C. L. T.; VIEIRA, F.; SAINT'PIERRE, T.D.; OLIVEIRA, A. C.; GONÇALVES, R. Direct determination of P in biodiesel by high-resolution continuum source graphite furnace atomic absorption spectrometry. **Spectrochimica Acta Part B**: Atomic Spectroscopy, v. 66, n. 5, p. 352-355, 2011.

OLIVEIRA, M. de; UESBECK, T.; GONÇALVES, T. S.; MAGON, C. J.; PIZANI P. S. de CAMARGO A. S. S.; ECKERT, H. Network structure and rare-earth ion local environments in fluoride phosphate photonic glasses studied by solid-state NMR and electron paramagnetic resonance spectroscopies. **The Journal of Physical Chemistry C**, v. 119, n. 43, p. 24574-24587, 2015.

EHRT, D.; CARL, M.; KITTEL, T.; MULLER, M.; SEEBER, W. High-performance glass for the deep ultraviolet range. **Journal of Non-Crystalline Solids**, v. 177, p. 405-419, 1994.

EHRT, D. Redox behaviour of polyvalent ions in the ppm range. **Journal of Non-Crystalline Solids**, v. 196, p. 304-308, 1996.

EHRT, D. Review: Phosphate and fluoride phosphate optical glasses — properties, structure and applications. **European Journal of Glass Science and Technology Part B**: Physics and Chemistry of Glasses, v. 56, n. 6, p. 217-234, 2015.

EHRT, D.; LEISTER, M.; MATTHAI, A. Polyvalent elements iron, tin and titanium in silicate, phosphate and fluoride glasses and melts. **Physics and Chemistry of Glasses**, v. 42, n. 3, p. 231-239, 2001.

EHRT, D.; SEEBER, W. Glass for high performance optics and laser technology. **Journal of Non-Crystalline Solids**, v. 129, n. 1/3, p. 19-30, 1991.

GULLION, T. Measurement of dipolar interactions between spin- 1 2 and quadrupolar nuclei by rotational-echo, adiabatic-passage, double-resonance NMR. **Chemical Physics Letters**, v. 246, n. 3, p. 325–330, 1995.

GUPTA, P. K. Non-crystalline solids: glasses and amorphous solids. **Journal of Non-Crystalline Solids**, v. 195, n. 1/2, p. 158-164, 1996.

JIANG, X.; JOLY, Y. N.; FINGER, A. M.; BABIC, F.; WONG, G. K. L.; TRAVERS, J. C.; RUSSEL, P. S. J. Deep-ultraviolet to mid-infrared supercontinuum generated in solid-core ZBLAN photonic crystal fibre. **Nature Photonics**, v. 9, n. 2, p. 133-139, 2015.

KALNINS, C. A. G.; HEIDEPRIEM, H. E.; DOWLER, A.; MONRO, T. M. Fabrication of fluoride phosphate glass optical fibres for UV applications. In: **INTERNATIONAL QUANTUM ELECTRONIC CONFERENCE; CONFERENCE LASERS ELECTRO-OPTICS**, Sydney, 2011. [Washington, DC]: AOS, 2011. p. 2051-2053. CD ROM.

KITAMURA, N.; HAYAKAWA, J.; YAMASHITA, H. Optical properties of fluoroaluminate glasses in the UV region. **Journal of Non-Crystalline Solids**, v. 126, n. 1/2, p. 155-160, 1990.

LUCAS, J.; SMEKTALA, F.; ADAM, J. L. Fluorine in optics. **Journal of Fluorine Chemistry**, v. 114, n. 2, p. 113-118, 2002.

MATTHAI, A.; EHRT, D.; RÜSSEL, C. Redox behaviour of polyvalent ions in phosphate glass melts and phosphate glasses. **Glass Science and Technology**, v. 71, n. 7, p. 187-192, 1998.

MIMURA, Y.; NAKAI, T. Optical fiber loss mechanisms. In: AGGARWAL, I. D.; LU, G. (Ed.). **Fluoride glass fiber optics**. NewYork: Elsevier, 1991. p. 235-274.

MÖNCKE, D.; EHRT, D.; VELLI, L. L.; VARSAMIS, C. P. E., KAMITSOS, E. I. Structure and properties of mixed phosphate and fluoride glasses. Physics and Chemistry of Glasses- **European Journal of Glass Science and Technology Part B**: v. 46, n. 2, p. 67-71, 2005.

NALIN, M.; RIBEIRO, S. J. L., MANZANI, D.; GONÇALVES, R. R.; POIRIER, G.; MATOS, C. J. S.; CASSANGES, F. C.; MENDONÇA, R. C.; BONI, L.; MISOGUTI, L.; MALTA, O.; LEDEMI, Y.; MESSADDEQ, S.; MESSADDEQ, Y. Glassy materials and light: part 1. **Química Nova**, v. 39, n. 3, p. 340-351, 2016.

OTO, M.; KIKUGAWA, S.; SARUKURA, N.; HIRANO, M.; HOSONO, H. Optical fiber for deep ultraviolet light. **IEEE Photonics Technology Letters**, v. 13, n. 9, p. 978-980, 2001.

PHILLIPS, C. J. **Glass, its industrial applications**. New York: Reinhold, 1960.

RAO, M. A Brief Introduction to Excimer Lasers: Fundamental Study. **International Journal of Advances in Pharmacy, Biology and Chemistry**, v. 2, n. 3, p. 533–536, 2013.

SKUJA, L.; HOSONO, H.; HIRANO, M.; KOICHI, K. Advances in silica-based glasses for UV and vacuum UV laser optics. **Proceedings of the SPIE**: the International Society for Optical Materials, v. 5122, p. 1-14, 2013.

VAN VLECK, J. H. The Dipolar Broadening of Magnetic Resonance Lines in Crystals. **Physical Review**, v. 74, p. 1168–1183, 1948.

VYDRA, J.; SCHOETZ, G. F. Improved all-silica fibers for deep-UV applications. **Proceedings of the SPIE**: the International Society for Optical Engineering, v. 3596, p. 165-175, 1999.

WANG, P.; LU, M.; GAO, F.; XU, Y.; HOU, C.; ZHOU,; Z. PENG, B. Luminescence in the fluoride-containing phosphate-based glasses: a possible origin of their high resistance to nanosecond pulse laser-induced damage. **Scientific Reports**, 2015. doi:10.1038/srep08593.

WELZ, B.; SPERLING, M. **Physical principles**: Atomic absorption spectrometry, 3rd ed. New Jersey: Wiley-VCH, 1998. 965 p.

WILLIAMS, R. T.; NAGEL, D. J.; KLEIN, P. H. Vacuum ultraviolet properties of beryllium fluoride glass. **Journal of Applied Physics**, v. 52, n. 10, p. 6279-6284, 1981.

ZARZYCKI, J. **Glasses and the vitreous state.** Cambridge: Cambridge University Press, 1991. 505 p.

ZOU, X.; ITOH, K.; TORATANI, H. Transmission loss characteristics of fluorophosphate optical fibers in the ultraviolet to visible wavelength region. **Journal of Non-Crystalline Solids**, v. 215, n. 1, p. 11-20, 1997.

ZOU, X.; TORATANI, H. Radiation resistance of fluorophosphate glasses for high performance optical fiber in the ultraviolet region. **Journal of Applied Physics**, v. 81, n. 8, p. 3354-3362, 2015.